mathematics

MDPI

Article

Numerical Investigation of Double-Diffusive Convection in an Irregular Porous Cavity Subjected to Inclined Magnetic Field Using Finite Element Method

Imran Shabir Chuhan [1,*], Jing Li [1], Muhammad Shafiq Ahmed [2], Inna Samuilik [3,4], Muhammad Aqib Aslam [5] and Malik Abdul Manan [6]

[1] Interdisciplinary Research Institute, School of Mathematics, Statistics and Mechanics, Beijing University of Technology, Beijing 100124, China; leejing@bjut.edu.cn
[2] Department of Mathematics and Physics, School of Arts and Science, American University of Ras al Khaimah, Ras al Khaimah 72603, United Arab Emirates; muhammad.ahmed@aurak.ac.ae
[3] Institute of Life Sciences and Technologies, Daugavpils University, 13 Vienibas Street, LV-5401 Daugavpils, Latvia; inna.samuilika@rtu.lv
[4] Institute of Applied Mathematics, Riga Technical University, LV-1048 Riga, Latvia
[5] Department of Mathematics, Faculty of Science, Beijing University of Technology, Beijing 100124, China; aqibaslam36@gmail.com
[6] Faculty of Information Technology, Beijing University of Technology, Beijing 100124, China; manansandila@emails.bjut.edu.cn
* Correspondence: imranshabbir1989@hotmail.com

Abstract: Purpose—This study aims to perform an in-depth analysis of double-diffusive natural convection (DDNC) in an irregularly shaped porous cavity. We investigate the convective heat transfer process induced by the lower wall treated as a heat source while the side walls of the enclosure are maintained at a lower temperature and concentration, and the remaining wall is adiabatic. Various factors, such as the Rayleigh number, Darcy effects, Hartmann number, Lewis number and effects of magnetic inclination are evaluated for their influence on flow dynamics and heat distribution. Design/methodology/approach—After validating the results, the FEM (finite element method) is used to simulate the flow pattern, temperature variations, and concentration by solving the nonlinear partial differential equations with the modified Rayleigh number ($10^4 \leq Ra \leq 10^7$), Darcy number ($10^{-4} \leq Da \leq 10^{-1}$), Lewis number ($0.1 \leq Le \leq 10$), and Hartmann number ($0 \leq Ha \leq 40$) as the dimensionless operating parameters. **Findings**—The finding shows that the patterns of convection and the shape of the isotherms within porous enclosures are notably affected by the angle of the applied magnetic field. This study enhances our understanding of how double-diffusive natural convection (DDNC) operates in these enclosures, which helps improve heating and cooling technologies in various engineering fields. **Research limitations/implications**—Numerical and experimental extensions of the present study make it possible to investigate differences in thermal performance as a result of various curvatures, orientations, boundary conditions, and the use of three-dimensional analysis and other working fluids. **Practical implications**—The geometry configurations used in this study have wide-ranging applications in engineering fields, such as in heat exchangers, crystallization, microelectronics, energy storage, mixing, food processing, and biomedical systems. **Originality/value**—This study shows how an inclined magnetic field affects double-diffusive natural convection (DDNC) within a porous system featuring an irregularly shaped cavity, considering various multiphysical conditions.

Keywords: double diffusive; MHD; irregular cavity; FEM

MSC: 65-XX

check for updates

Citation: Chuhan, I.S.; Li, J.; Ahmed, M.S.; Samuilik, I.; Aslam, M.A.; Manan, M.A. Numerical Investigation of Double-Diffusive Convection in an Irregular Porous Cavity Subjected to Inclined Magnetic Field Using Finite Element Method. *Mathematics* **2024**, *12*, 808. https://doi.org/10.3390/math12060808

Academic Editor: Alicia Cordero

Received: 26 February 2024
Revised: 7 March 2024
Accepted: 8 March 2024
Published: 9 March 2024

Copyright: © 2024 by the authors. Licensee MDPI, Basel, Switzerland. This article is an open access article distributed under the terms and conditions of the Creative Commons Attribution (CC BY) license (https://creativecommons.org/licenses/by/4.0/).

1. Introduction

Double-diffusive natural convection (DDNC) refers to the combined effects of buoyancy-driven fluid flow and the simultaneous transport of heat and mass. Different flow patterns and convective cells develop in DDNC fluids due to buoyancy forces caused by temperature and concentration variations. There are several uses for natural convection, including in geothermal systems [1,2], chemical engineering, crystal formation, and separation processes [3,4]. Natural convection is the movement of fluid driven by buoyancy force due to mass and heat transfer. In engineering applications, natural convection is important for cooling systems, sun collectors, and many other thermal devices that need to move heat efficiently. Natural convection is a fundamental mechanism for heat transfer in geothermal systems, as the heat is transferred from the hotter regions to the cooler regions, and buoyancy forces are generated, leading to the formation of convective cells and flow patterns. This phenomenon has numerous industrial applications and natural processes including contaminant transport [5,6], drying methods [7], and chemical reactors [8]. An irregular cavity can further complicate the natural convection patterns in geothermal systems, resulting in complex flow and heat transfer phenomena. The interplay between natural convection and the irregularities of the cavity can have an important impact on the efficiency and performance of the system. The complex interplay between heat and mass transfer, porous effects, and irregular cavities has generated significant interest among researchers in various fields, from geothermal systems to chemical engineering. Numerous studies have examined cavities of varying shapes, such as, trapezoids [9,10], triangles [11–13], irregular wall cavities [14], and more unusual shapes [15]. Izadi et al. [16] conducted a detailed discussion on mixed convection in enclosures of various shapes and summarized the key findings regarding the enhancement of heat transfer and the effects on pumping power. The dynamics of fluid movement and thermal conduction in these cavities and how they are affected by their shape were the focus of these analyses. All the above studies conclude that the Soret and Dufour effects are two critical physical phenomena that significantly influence the thermal, diffusive transport characteristics and the fluid flow behavior in DDNC. The study of thermal and diffusive transport characteristics in porous media under DDNC was first initiated by Bejan et al. [17]. They analyzed the effect of Lewis numbers in a porous medium. Later on, Goyeau et al. [18] analyzed an enclosure filled with a saturated porous medium and applied the Darcy–Brinkman model to describe the flow within it. They investigated the impact of porosity and Darcy's number on double-diffusive natural convection (DDNC) within the porous cavity. The simulation findings from their study indicated that while the influence of porosity on the heat and mass transfer rate was negligible at low Darcy numbers, a higher porosity significantly increased the rates of thermal energy transfer and mass transport at high Darcy numbers. Mondal et al. [19] investigated non-steady-state DDNC in porous media and examined the variation in the buoyancy ratio on heat and mass transfer rate. Chamkha et al. [20] studied DDNC in a tilted porous cavity using the finite difference method (FDM). Their results demonstrated that thermal and diffusive transport is affected not only by Darcy's number and the buoyancy ratio but also by the tilt angle and aspect ratio of a square cavity. Moreover, porous media in cavities used in industrial production are often accompanied by a composite layer. Numerical research on DDNC in a porous cavity with irregular porosity was discussed by He et al. [21], which comprised two parallel porous layers having distinct porosity levels. The investigation conducted by Vijaybabu et al. [22] focused on analyzing the influence of MHD (magnetohydrodynamic) and porous circular cylinders on DDNC and an irreversibility analysis within an enclosure. The researcher Astanina et al. [23] focused on thermogravitational convection in a porous cube with a non-uniform heating of the vertical wall. The mathematical modeling of fluid flow in the heated center of a wavy-shaped cavity as discussed by Rashid et al. [24], focusing on the thermal and diffusive transport in a MHD Casson fluid flow. This study is part of the significant attention given to DDNC in various fields, such as oceanography, metallurgy, and astrophysics.

Magnetohydrodynamics is an important physical phenomenon that has garnered a lot of interest due to its numerous applications in various fields, including engineering and environmental sciences. Numerous studies have investigated the influence of magnetohydrodynamics on heat transfer in enclosures to assess the impact of magnetic fields on heat transfer, whether it occurs via conduction or convection. An FEM was investigated by Rahman et al. [25] to explore the combined impact of magnetohydrodynamics and joule heating on DDNC within a horizontal channel featuring an open enclosure. Teamah et al. [26] explored the effects of the magnetic field and heat source on the DDNC flow in a rectangular enclosure. The researchers observed that increasing the magnetic field resulted in a decrease in fluid circulation and thermal and diffusive transport rates within the cavity. Kumar et al. [27] studied the thermal and diffusive transport in the 2D MHD free convection process, considering the thermal diffusion. The process occurred in a Darcy porous enclosure in a stratified thermal and mass fluid. Bayareh et al. [28] explored the effects of magnetic fields on the thermodynamic efficiency of nanofluid-filled cavities, detailing the role of AI in optimizing system performance and forecasting future advancements. Seyyedi et al. [29] discussed natural convection and entropy generation within a square inclined cavity affected by magnetohydrodynamic (MHD) forces, revealing peaks in entropy generation at specific inclination angles and Hartmann numbers. Ali et al. [30] explained the MHD behavior of mixed convection in a hexagonal enclosure.

The main objective of this research is to investigate the heat and mass transfer in an irregularly shaped porous cavity using the finite element method. To the best of our knowledge, based on a thorough literature review, there are no studies on irregularly shaped enclosures using hybrid mesh techniques. The hybrid mesh consists of both triangular and rectangular shapes. The novelty of the work lies in how an inclined magnetic field influences double-diffusive natural convection (DDNC) within a porous system with an irregularly shaped cavity, taking into account various multiphysical conditions. Therefore, various parameters can be utilized to control heat and mass transfer. This study has applications in heat exchangers, crystallization, microelectronics, food processing, and biomedical systems.

2. Mathematical Formulation

The domain analyzed in this study is a two-dimensional, irregular enclosure with a fluid-permeated porous medium, assumed to be incompressible and steady, and subjected to an inclined magnetic field, as shown in Figure 1. The porous medium contains a mixture of an inert fluid and a solute, which undergoes mass transfer. The side walls and horizontal walls of the cavity are maintained at different constant concentrations and temperatures, resulting in a DDNC problem. The lowest concentration and temperature are along the side walls and the highest ones along the horizontal wall. The enclosure's upper wall is adiabatic.

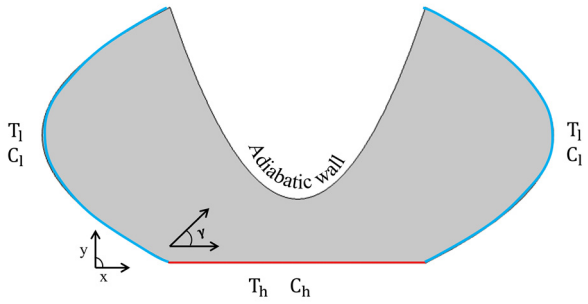


Figure 1. Sketch view of the model.

Governing Equations

Considering the above assumptions, the dimensional equations for continuity, momentum, energy, and concentration can be shown as [31].

$$\frac{\partial u}{\partial x} + \frac{\partial v}{\partial y} = 0 \tag{1}$$

$$\rho\left(u\frac{\partial u}{\partial x} + v\frac{\partial u}{\partial y}\right) + \frac{\partial p}{\partial x} = \mu\left(\frac{\partial^2 u}{\partial x^2} + \frac{\partial^2 u}{\partial y^2}\right) - \frac{\mu}{K}u + \xi_x \tag{2}$$

$$\rho\left(u\frac{\partial v}{\partial x} + v\frac{\partial v}{\partial y}\right) + \frac{\partial p}{\partial y} = \mu\left(\frac{\partial^2 v}{\partial x^2} + \frac{\partial^2 v}{\partial y^2}\right) - \frac{\mu}{K}v + \xi_y \tag{3}$$

where ξ_x and ξ_y represent force terms called the Boussinesq approximation and magnetic field, which contain

$$\xi_x = -\varrho B_0^2\left(u{\cdot}sin^2\gamma - v{\cdot}sin\gamma cos\gamma\right)$$

$$\xi_y = -\varrho B_0^2\left(v{\cdot}cos^2\gamma - u{\cdot}cos\gamma sin\gamma\right) + \rho g[\beta_T(T - T_l) + \beta_c(c - c_l)]$$

$$\frac{1}{\varsigma}\left(u\frac{\partial T}{\partial x} + v\frac{\partial T}{\partial y}\right) = \left(\frac{\partial^2 T}{\partial x^2} + \frac{\partial^2 T}{\partial y^2}\right) \tag{4}$$

$$\frac{1}{D}\left(u\frac{\partial c}{\partial x} + v\frac{\partial c}{\partial y}\right) = \left(\frac{\partial^2 c}{\partial x^2} + \frac{\partial^2 c}{\partial y^2}\right) \tag{5}$$

ς is a diffusion coefficient and D is the magnetic diffusivity.

To convert the dimensional equations into a nondimensional form, the following dimensionless parameter were used [32,33]:

Dimensionless parameter	Definition
Rayleigh number	$Ra = \frac{\rho^2\beta_T g H^3 \Delta T Pr}{v^2}$
Lewis number	$Le = \frac{\varsigma}{D}$
Prandtl number	$P_r = \frac{v}{a}$
Darcy number	$Da = \frac{K}{H^2}$
Hartmann number	$Ha = BH\sqrt{\frac{\varrho}{\mu}}$
Temperature	$\theta = \frac{(T - T_l)}{(T_h - T_l)}$
Fluid pressure	$P = \frac{p}{\rho\alpha^2}$
Velocity	$U = \frac{uH}{\alpha}, V = \frac{vH}{\alpha}$

The dimensionless form of Equations (1)–(5) are

$$\frac{\partial U}{\partial X} + \frac{\partial V}{\partial Y} = 0 \tag{6}$$

$$U\frac{\partial U}{\partial X} + V\frac{\partial U}{\partial Y} + \frac{\partial P}{\partial X} = P_r\left(\frac{\partial^2 U}{\partial X^2} + \frac{\partial^2 U}{\partial Y^2}\right) - \frac{P_r}{Da}U + \xi_X, \tag{7}$$

$$U\frac{\partial V}{\partial X} + V\frac{\partial V}{\partial Y} + \frac{\partial P}{\partial Y} = P_r\left(\frac{\partial^2 V}{\partial X^2} + \frac{\partial^2 V}{\partial Y^2}\right) - \frac{P_r}{Da}V + \xi_Y \tag{8}$$

where $P_r = \frac{\mu}{\rho}$

$$\xi_X = Ha^2 P_r\left(sin\gamma cos\gamma\, V - sin^2\gamma U\right),$$
$$\xi_Y = Ha^2 P_r\left(sin\gamma cos\gamma\, U - cos^2\gamma\, V\right) + P_r Ra(NC + \theta)$$

$$U\frac{\partial\theta}{\partial X}+V\frac{\partial\theta}{\partial Y}=\left(\frac{\partial^2\theta}{\partial X^2}+\frac{\partial^2\theta}{\partial Y^2}\right) \tag{9}$$

$$Le\left(U\frac{\partial C}{\partial X}+V\frac{\partial C}{\partial Y}\right)=\left(\frac{\partial^2 C}{\partial X^2}+\frac{\partial^2 C}{\partial Y^2}\right) \tag{10}$$

The dimensionless boundary conditions are

Cold wall	$C=0, \theta=0$	$U=0,\ V=0$
Hot wall	$C=1, \theta=1$	$U=0,\ V=0$
Remaining wall	$C_n=0.\ \theta_n=0$	$U=0,\ V=0$

The average values in question can be determined by performing an integration over the heated section.

The averaged Nusselt number is

$$Nu_{av}=\int_0^1 Nu\ dY \tag{11}$$

The averaged Sherwood Number is

$$Sh_{av}=\int_0^1 Sh\ dY \tag{12}$$

The local Nusselt number Nu_{lo} and local Sherwood Number Sh_{lo} are computed through the equation

$$Nu_{lo}=-\left(\frac{\partial\theta}{\partial n}\right)_s \tag{13}$$

$$Sh_{lo}=-\left(\frac{\partial C}{\partial n}\right)_s \tag{14}$$

where (s) refers to the surface of the region, and (n) represents the normal direction to the surface.

In addition, the kinetic energy (total) is

$$K.E.=\frac{1}{2}\int_\Omega \|U\|^2 d\Omega \tag{15}$$

3. Numerical Methodology

Several computational techniques have been developed to determine the dynamics of fluid movement and heat transfer rates in different types of enclosures. In this investigation, the FEM is utilized to discretize and solve Equations (6)–(10) along with their corresponding boundary conditions [34,35]. The FEM is acknowledged as a highly efficient computational scheme for obtaining optimized solutions. The research carried out by [36] focused on comparing the FVM and the FDM for the simulation of lid-driven cavity flow. The finite element approach creates a discrete nonlinear system of equations by discretizing equations using a weak formulation. The resulting nonlinear system is solved using the Newton method, whereas the linear inner system is solved directly using the PARDISO program. LU matrix factorization is used in the solver to improve computational efficiency and reduce the required iterations for convergence, resulting in faster and more accurate solutions for complex systems of equations. The iterative process, combined with discretization techniques, greatly reduces the required iterations for obtaining accurate solutions, enhancing computational efficiency. The finite element method employs variable-specific discretization schemes: a second-order one for velocity elements and a linear-order one for temperature and solute concentration, optimizing accuracy and computational efficiency. This approach yields optimized solutions and enhances the understanding of the underlying physics. The computational domain is discretized using a non-uniform mesh comprising triangular and rectangular elements, enabling a flexible representation of

irregular geometries. To ensure accuracy in critical areas, a higher density of mesh points is allocated. Figure 2 illustrates the combined use of rectangular and triangular elements in the hybrid finite element grid. This hybrid mesh configuration effectively balances accuracy and computational efficiency, thereby enhancing solution precision. Prior to simulating the model under consideration, the current code was first tested by applying it to previously reported models. The grid independence was established, and the code's validation was demonstrated through a comparison of the average Nusselt number with the findings from [32,37], using $Ha = 25$, $Le = 2.5$, $Pr = 6.8$, $Ra = 10^5$, and various β values as outlined in Table 1. The results are in Figure 3, demonstrating the effectiveness and applicability of the current code. Figure 4 represents the systematic approach employed to implement the proposed methodology.

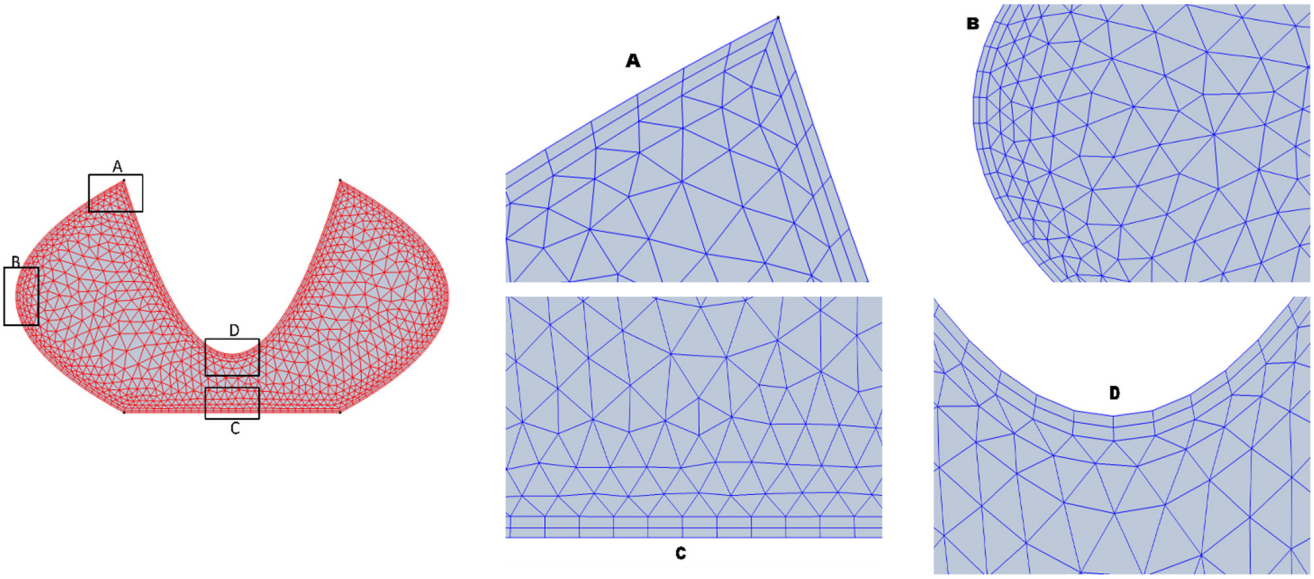


Figure 2. Mesh analysis at different positions, highlighting the specific mesh region (**A**–**D**).

Table 1. Comparison of average Nusselt number for $Ha = 25$, $Ra = 10^5$, $Pr = 6.8$, $Le = 2.5$ with previous studies for different values of β.

β	[37]	[32]	**Present**
0.1	2.39023	2.38986	2.2821
1	3.81168	3.81194	3.7710
5	4.27511	4.27587	4.2651
10	4.35470	4.35556	4.3120

Grid Convergence

To evaluate the impact of grid configuration on simulation results, it is an essential step to investigate the correlation between the number of grid points and Nu_{avg}. To achieve this, the impact of different grid points on the averaged Nusselt number was evaluated for $Ha = 25$, $Ra = 10^5$, $\gamma = 0^o$, $Le = 0.1$, $Da = 0.1$ at an extrafine level. It was observed that any grid structure was finer when Nu_{avg}, Sh_{avg}, and $K.E.$ remained constant, as shown in Table 2. As a result, we chose a uniform grid of level 8.

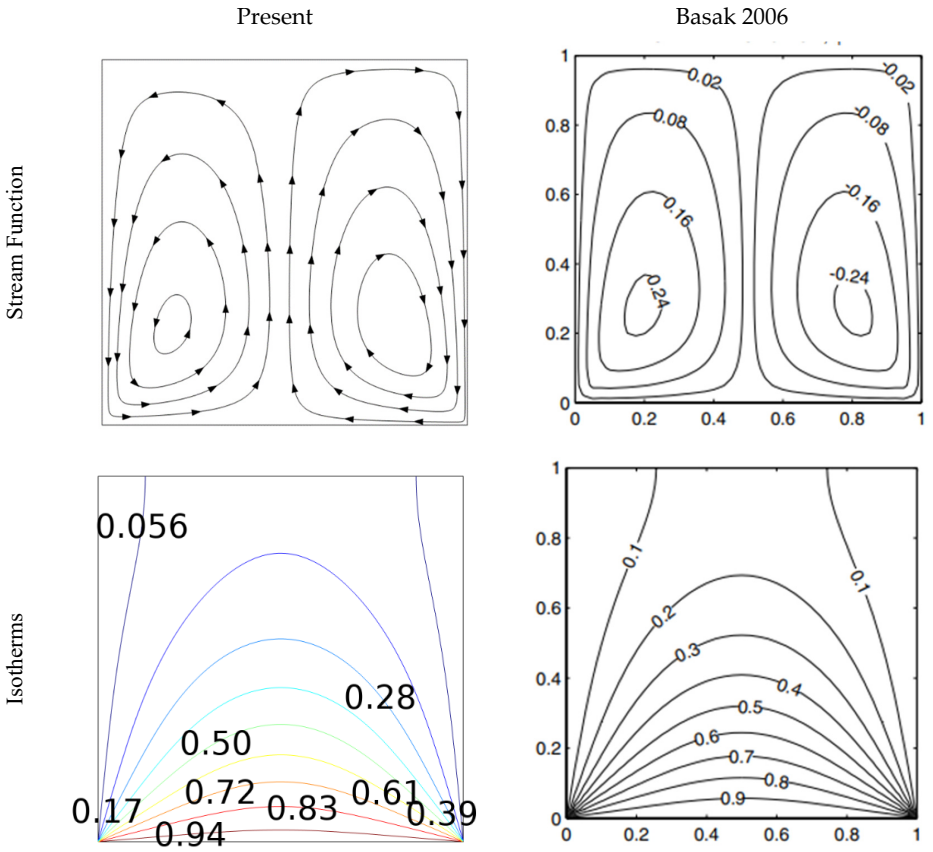


Figure 3. Comparison of the results with Basak et al. [38] in terms of streamlines and isotherms; $P_r = 0.71$ and $Ra = 10^6$, $Da = 10^{-5}$.

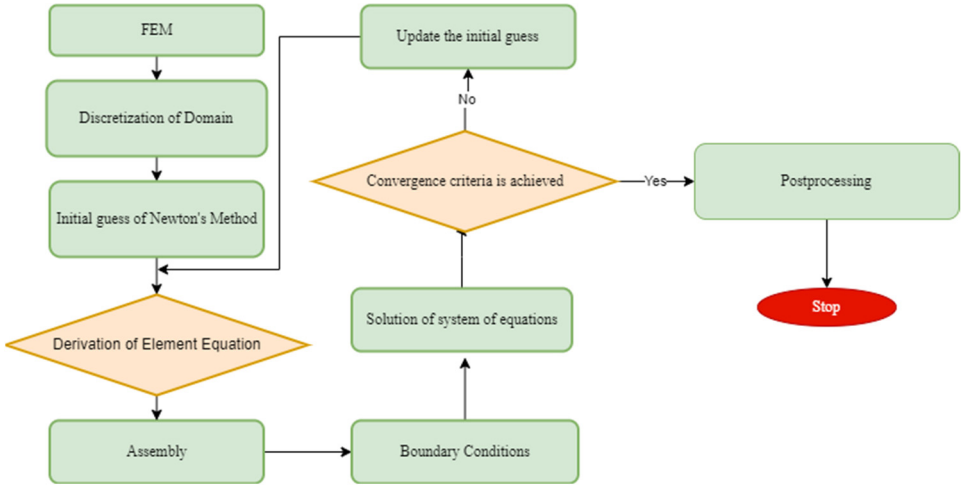


Figure 4. FEM flow chart.

Table 2. Grid independence tests for Nu_{avg} for $Ra = 10^5, \gamma = 0^o, Ha = 25, Le = 0.1, Da = 0.1$.

Grid	NEL	DOFs	Nu_{avg}	Error [%]
Fine	3352	32076	7.31940	7.69
Finer	9516	88550	7.88235	5.91
Extrafine	24908	226590	8.37816	0.003
Extremely Fine	34284	306286	8.37847	

4. Result and Discussions

This section presents a detailed analysis of the numerical investigation conducted on natural convection in a 2D laminar flow regime within an irregular enclosure under Darcy's impact. The results are compiled by examining the impact of the Hartmann number $0 \leq Ha \leq 40$, Darcy number ($10^{-4} \leq Da \leq 10^{-1}$), Lewis number ($0.1 \leq Le \leq 10$), and Rayleigh number ($10^4 \leq Ra \leq 10^7$) on the flow. The streamlines, isotherms, and isoconcentration are presented.

4.1. Impact of Rayleigh's Number

Figure 5 shows contour maps of velocity streamlines, isotherms, and isoconcentration for different Rayleigh numbers in the range $10^4 \leq Ra \leq 10^7$ at $Ha = 25$, $Le = 0.1$, $Da = 0.1$. At lower Rayleigh numbers, the flow is stable and streamlined, with evenly spaced isotherms and isoconcentration lines indicating a uniform heat and mass distribution. As the Rayleigh number increases, the streamlines become more complex, indicating a transition from stable laminar flow to a more dynamic regime, possibly approaching turbulence. This is further evidenced by the increasingly intricate isotherm and isoconcentration patterns, suggesting enhanced fluid mixing. The temperature remains the highest at the lower wall and the lowest at the side walls, consistent with the imposed boundary conditions, while the adiabatic upper wall shows no temperature change due to its insulation. The plots indicate that as the Rayleigh number (Ra) increases, buoyancy forces grow stronger, shifting the dominant heat transfer mechanism from conduction to convection. This results in improved thermal mixing and convection, which can impact the effectiveness of thermal systems such as heat exchangers and cooling units. Figure 6 represents the impact of Ra on the averaged Sherwood number, averaged Nusselt number, and total kinetic energy. Apparently, Nu_{avg} and Sh_{avg} rises with Ra, and the maximum values of Nu_{avg}, Sh_{avg} and $K.E$ are 14.5, 32 and 8×10^3 for $10^4 \leq Ra \leq 10^6$.

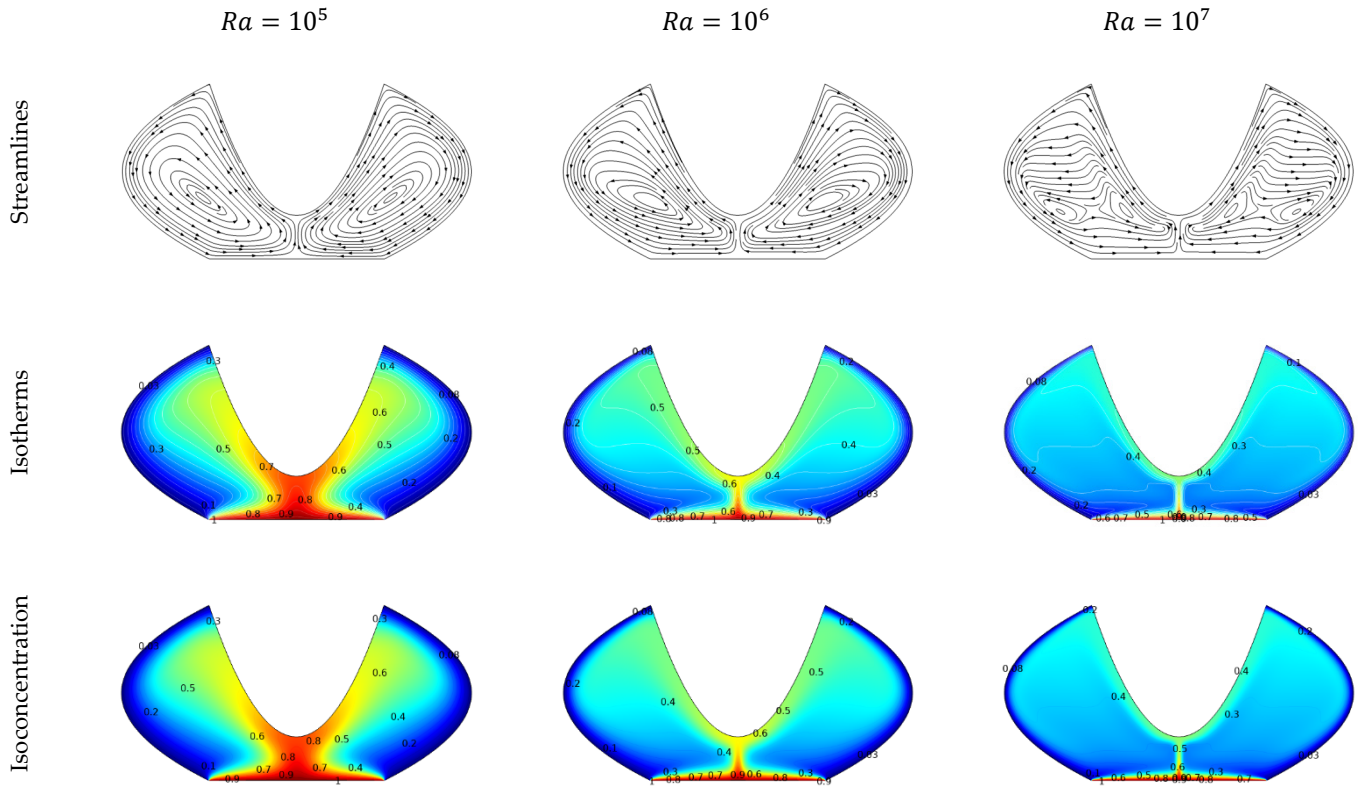


Figure 5. Variations in flow dynamics, temperature fields, and solute dispersion depicted through streamlines, isotherms, and isoconcentration profiles across different Rayleigh numbers (Ra).

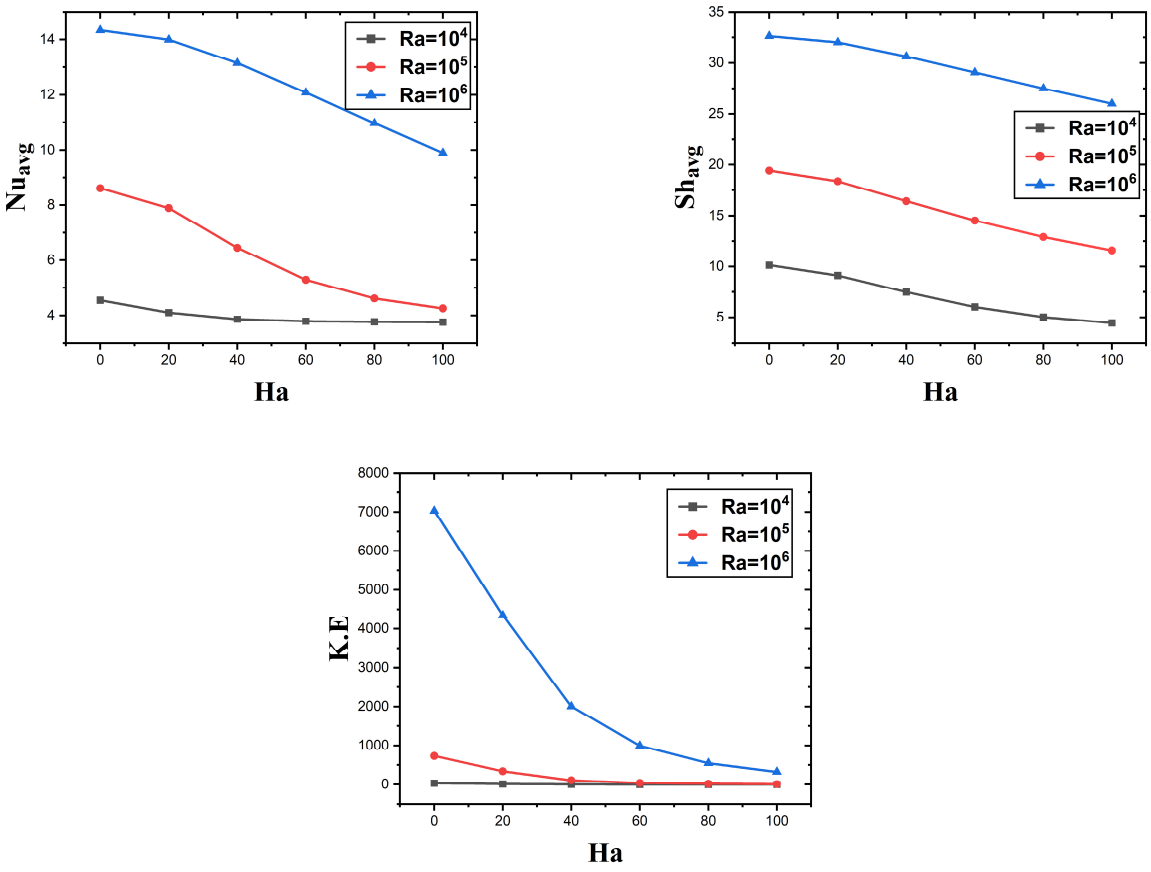


Figure 6. The graph displays the impact of Ra on the average Nusselt number, average Sherwood number, and total kinetic energy.

4.2. Impact of Lewis's Number

The effect of varying Le $(1 \leq Le \leq 10)$ on momentum, isotherms, and isoconcentration is illustrated in Figure 7. It demonstrates that there is no considerable change in momentum when the Lewis number increases because it is not directly associated with diffusion. The fluid rotates clockwise due to the lower wall being heated, and the side walls have a minimum temperature. At low Lewis numbers, the flow exhibits smooth velocity streamlines with uniform isoconcentration and isotherm contours, indicating a balanced distribution of concentration and temperature. As Le increases, the flow becomes more complex, characterized by intricate velocity streamlines that signify enhanced fluid mixing and convection. Consequently, the flow pattern becomes highly irregular, resulting in improved convective transport within the system. High Lewis numbers increase thermal diffusivity relative to mass diffusivity. The fluid concentration distribution may change. Fluid concentrations on the hot side increase with the Lewis number. Figure 8 illustrates that when Le increases, the mean Nusselt number increase for $0.1 \leq Le \leq 1$, and the heat transfer rate decreases for $1 \leq Le \leq 5$.

Table 3 represents the numerical values of Nu_{avg}, Sh_{avg}, and $K.E.$ for the parameters $Ha = 25$, $Le = 1$, $Da = 0.02$, $\gamma = 0^o$, $Ra = 10^5$. When Le increaes, the number Nu_{avg} and $K.E.$ decrease, but the mass transfer rate increases. For a low Hartmann number, Nu_{avg}, Sh_{avg}, and $K.E.$ have their maximum value when the Ha mass transfer rate, the heat transfer rate, and total energy decrease. This table also shows that the value of Nu_{avg}, Sh_{avg}, and $K.E.$ increases with increasing Da, γ, and Ra.

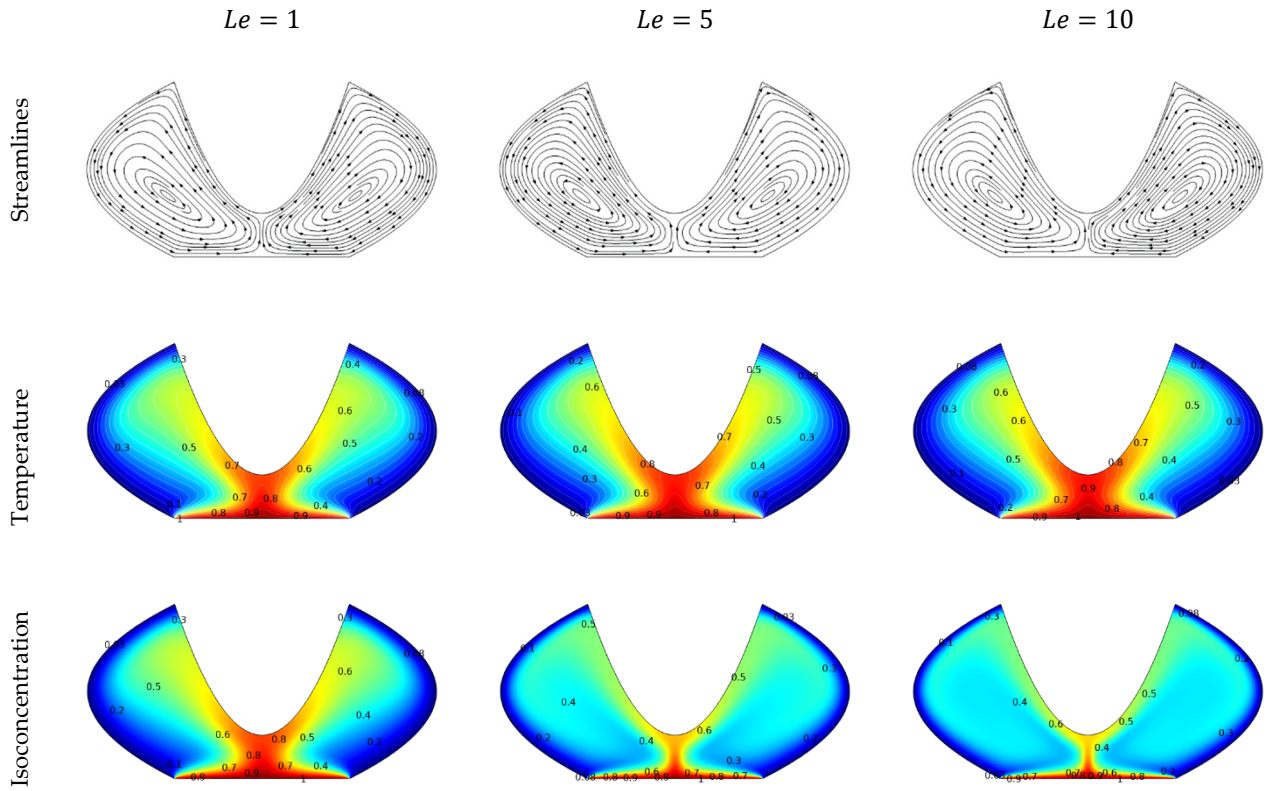


Figure 7. Flow patterns, thermal distribution, and concentration fields within an enclosure for different Lewis numbers (*Le*), displaying streamlines, temperature contours and concentration distributions.

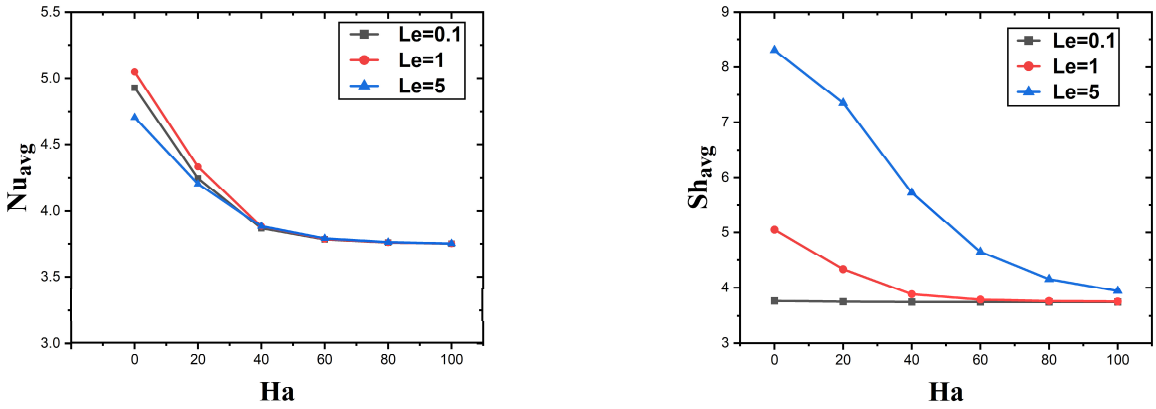


Figure 8. The graph displays the impact of *Le* on the Nusselt number (averaged) and Sherwood number (averaged).

Table 3. Comparative numerical values of Nusselt number (averaged), Sherwood number (averaged), and kinetic energy (total) for various physical parameters.

Le	γ	*Ra*	*Da*	*Ha*	Nu_{avg}	Sh_{avg}	*KE*
1	0^o	10^5	0.02	25	9.9430	9.9441	523.8414
0.1	-	-	-	-	9.9034	5.2336	647.8792
5	-	-	-	-	9.0698	15.6499	294.8795
10	-	-	-	-	8.7665	19.0674	253.2713
-	15^o	-	-	-	9.3401	9.3413	439.5714

Table 3. *Cont.*

Le	γ	*Ra*	*Da*	*Ha*	Nu_{avg}	Sh_{avg}	*KE*
-	30°	-	-	-	9.3477	9.3488	471.8329
-	45°	-	-	-	9.9732	9.9744	612.1477
-	-	10^3	-	-	4.9731	4.9741	0.0700
-	-	10^4	-	-	5.3781	5.3791	10.6999
-	-	10^6	-	-	16.4802	16.4821	6513.5956
-	-	-	0.0002	-	5.3800	5.3810	9.2370
-	-	-	0.002	-	8.5885	5.5896	229.3243
-	-	-	0.2	-	10.1091	10.1103	587.1623
-	-	-	-	0	10.8920	10.8923	1366.3958
-	-	-	-	50	8.1211	8.1222	134.800
-	-	-	-	75	6.6340	6.6351	38.6461
-	-	-	-	100	5.7814	5.7824	13.1207

4.3. Impact of Darcy's Number

The streamlines, isoconcentration, and isotherms for various value of *Da* (0.0001, 0.001, 0.01) at $(Ha = 25,\ Le = 0.1,\ Ra = 10^5)$ are presented in Figure 9 for an irregular enclosure. Figure 9 shows how the Darcy number (*Da*) affects an enclosure's flow, heat, and mass transfer. As *Da* increases, the streamlines show more dynamic flow, indicating reduced flow resistance. The isotherms transition from tightly packed at low *Da* to more dispersed at high Da, suggesting enhanced thermal mixing.

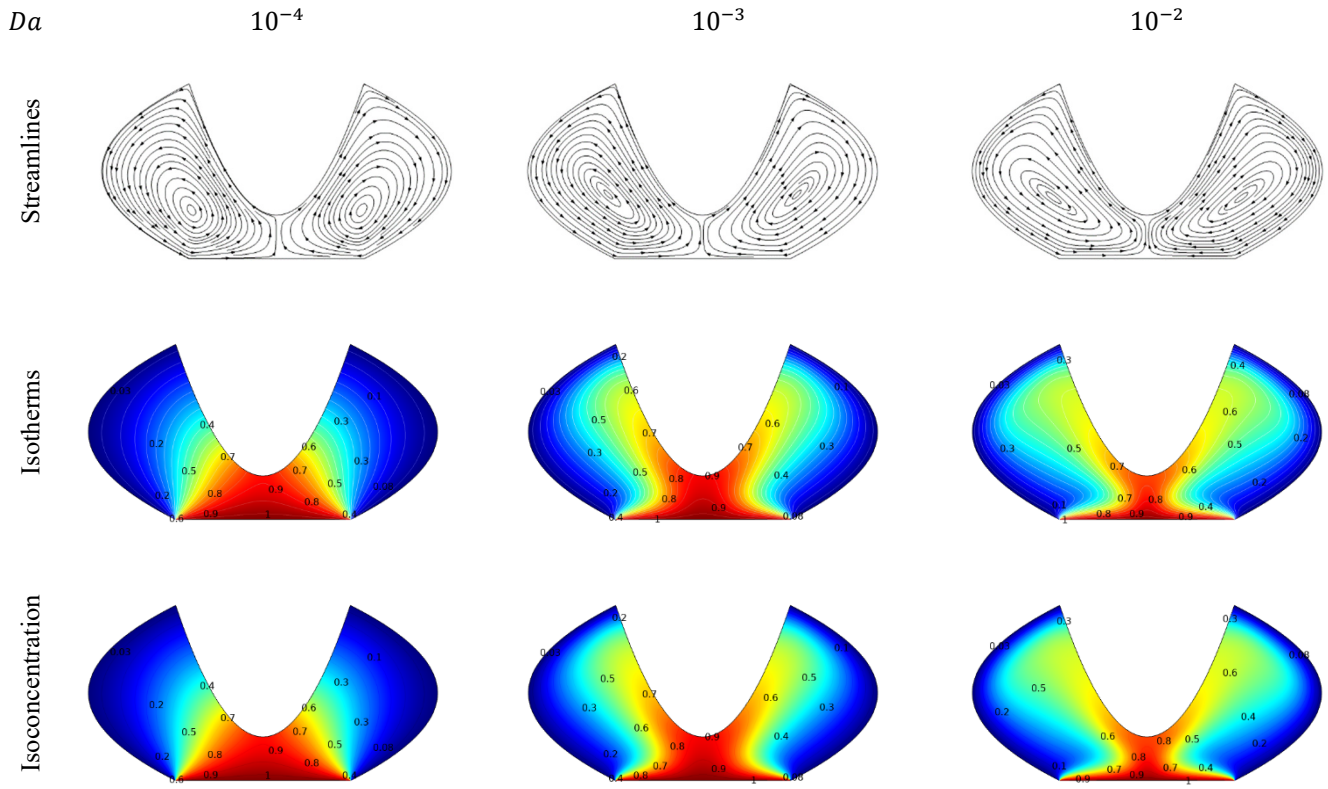


Figure 9. The figure represents the impact of Darcy's number on velocity streamlines, isotherms, and isoconcentrations.

The isoconcentration contours also become less stratified with a higher Da, reflecting better solute mixing. These changes reveal that a higher Da, indicative of a more permeable medium, promotes more effective heat and mass transfer, important for the design of porous media systems. In engineering applications, a high *Da* might be beneficial in processes requiring efficient thermal management, while a low *Da* might be desirable where minimal mixing is needed to maintain concentration gradients. Figure 10 illustrates the impact of Darcy's number on heat transfer rate and mass transfer rate. It can be seen that when the Darcy number rises, the mass transfer rate and heat transfer rate will increase.

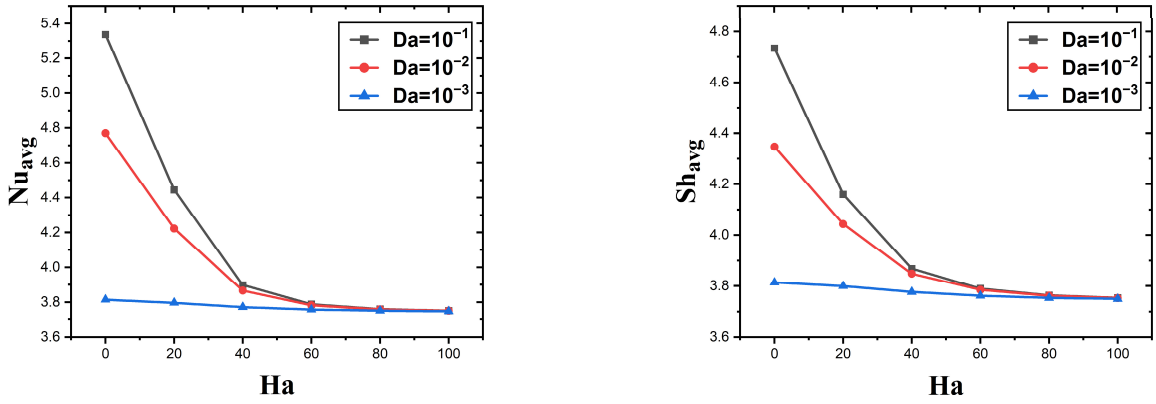


Figure 10. The graph displays the impact of *Da* on the Nusselt number (averaged) and Sherwood number (averaged).

4.4. Impact of Inclined Angle

Figure 11 demonstrates streamlines, isoconcentration, and isotherms for distinct values of the inclination angle γ with $Ha = 25$, $Ra = 10^5$, $Le = 0.1$, $Da = 0.1$. From Figure 11, the flow pattern inside the cavity can be described by a series of counterclockwise convection vortices. Temperatures rise on hot walls with an increasing inclined angle in isothermal systems. When the inclined angle increases, the concentration becomes more spread out and diffuse. The angle of inclination significantly influences the thermal efficiency and fluid dynamics in systems utilizing magnetic fields, impacting applications ranging from magnetic refrigeration to chemical processing. Designing enclosures, particularly for cooling systems, demands careful consideration of the inclination angle to optimize thermal control and maintain precise temperature gradients.

4.5. Impact of Hartmann's Number

Streamlines, isotherms, and isoconcentration distributions for different Hartmann numbers (*Ha*) are shown in Figure 12. The existence of a magnetic field makes Ha an important factor, due to the fact that it reduces the velocity profile and promotes a laminar flow phase. Hartmann's number is written as $Ha = BH\sqrt{\frac{\varrho}{\mu}}$. An increase in the value of *Ha* typically leads to the Lorentz force damping the fluid motion, which can suppress turbulence and result in a more uniform and potentially laminar flow structure. This may lead to a more uniform temperature distribution and a reduction in kinetic energy. In terms of concentration, an increase in Hartmann number can lead to a decrease in concentration gradients as the flow becomes more laminar.

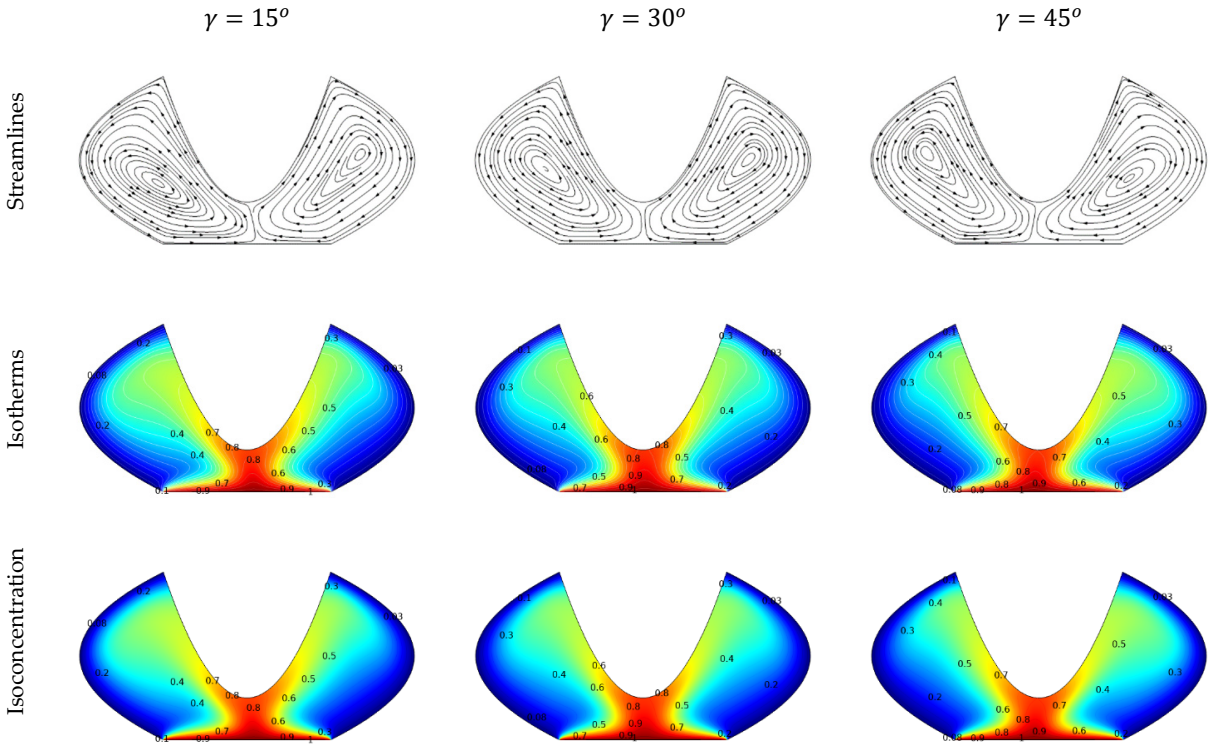


Figure 11. Effect of varying inclined angle (γ) on the flow structure, temperature distribution, and concentration levels within an enclosure, depicted through streamlines, isotherms, and isoconcentration contours.

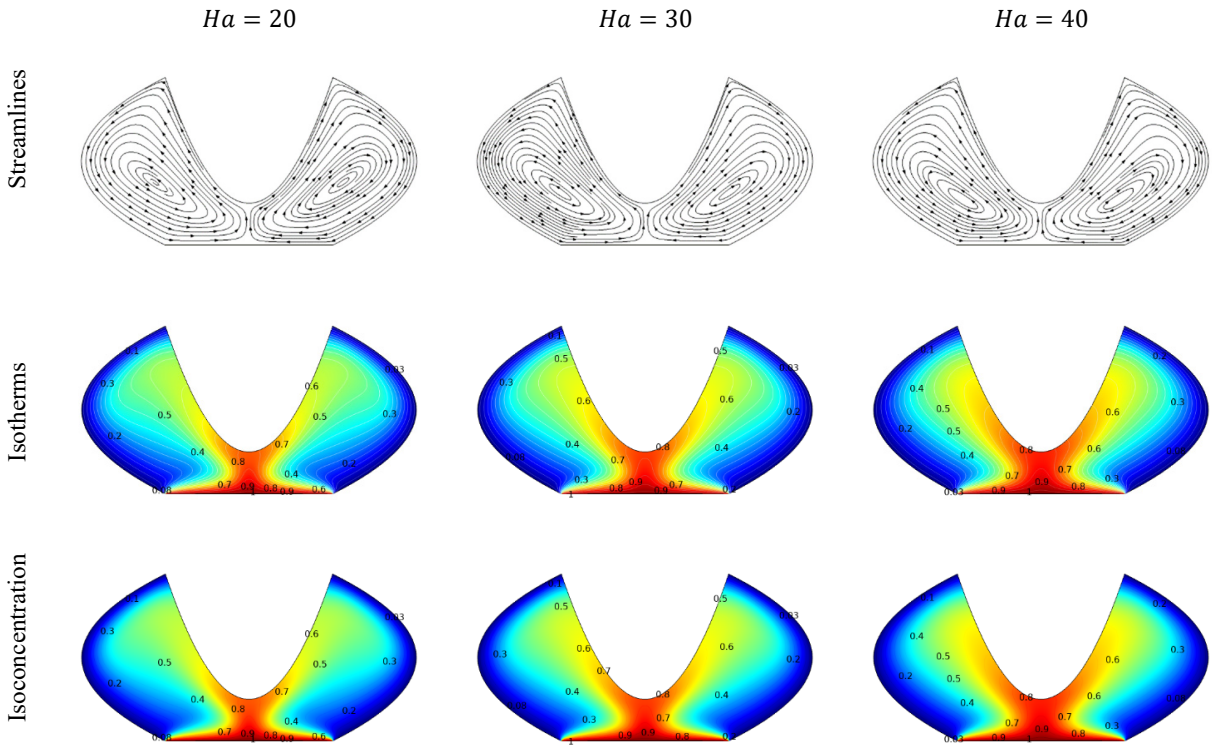


Figure 12. Influence of an increasing Hartmann number (*Ha*) on fluid motion, thermal stratification, and concentration distribution within an enclosure, presented through streamlines, isotherms, and isoconcentration plots.

5. Conclusions

In this study, the behavior of DDNC in an irregular cavity was explored and investigated. The investigation demonstrated that the flow characteristics were considerably influenced by the thermophysical properties of the fluid. The study also revealed that the inclination angle, Hartmann number, Lewis number, and Rayleigh number affected the flow, magnetic effects, heat transfer, and mass transfer in the cavity. The numerical analysis demonstrated that the flow inside the cavity is 2D and incompressible. This investigation provides significant insights into the behavior of DDNC in an irregular cavity, which could be useful for various engineering applications. The major outcomes of this investigation include the following:

- The heat transfer rate, mass transfer rate, and total kinetic energy increase with the rise in the Rayleigh number.
- In a specific range, $0.1 \leq Le \leq 1$, when the Lewis number rises, the mean Nusselt number and total energy decrease, but the mean Sherwood number increases.
- As the Rayleigh number increases, the isotherms and isoconcentration lines become more distorted, the concentration and temperature gradients become steeper. With the formation of plumes and vortices, the flow becomes more turbulent and complex.
- The findings indicate that the velocity of fluid flow decreases because of porous media flow resistance increasing the Darcy number. The velocity lines of the fluid become more densely packed, resulting in a more laminar flow.
- Nu_{avg}, Sh_{avg}, and *K.E.* increase when the Darcy number rises.
- The flow pattern within the cavity can be described by a series of counterclockwise convection vortices, and temperatures rise on hot walls with the increases in the inclined angle.

Author Contributions: Conceptualization, I.S.C.; methodology, I.S.C. and M.A.A.; validation, J.L. and I.S.; investigation, M.S.A.; writing—original draft preparation, I.S.C.; writing—review and editing, M.S.A.; supervision, J.L. and I.S.C.; project administration, M.A.M.; funding acquisition, I.S. All authors have read and agreed to the published version of the manuscript.

Funding: This research received no external funding.

Data Availability Statement: No new data were created or analyzed in this study. Data sharing is not applicable to this article.

Conflicts of Interest: The authors have no conflict of interest.

Nomenclature

B_0	Magnetic field strength (Tesla)	N	Buoyancy ratio
B	Magnetic field (Tesla)	NEL	Number of elements
c_p	Specific heat $\left(\mathrm{J{\cdot}Kg^{-1}{\cdot}K^{-1}}\right)$	P	Fluid pressure
c	Concentration $\left(\mathrm{Kgm^{-3}}\right)$	Pr	Prandtl's number
Da	Darcy's number	Ra	Rayleigh's number
DOF	Degree of freedom	Sh	Sherwood's number (local)
g	Gravity (m/s)	T	Temperature (K)
Ha	Hartmann's number	u, v	Velocity (x and y axis) $\left(\mathrm{m{\cdot}s^{-1}}\right)$
$K.E$	Total kinetic energy (J)	x, y	x and y coordinate (m)
Le	Lewis's number	γ	Angle (inclination) (rad)
M	Kinematic viscosity $\left(\mathrm{m^2{\cdot}s^{-1}}\right)$	ρ	Fluid density $\left(\mathrm{kg{\cdot}m^{-3}}\right)$
Nu	Nusselt number (local)	θ	Temperature

References

1. Turner, J. Double-diffusive phenomena. *Annu. Rev. Fluid Mech.* **1974**, *6*, 37–54. [CrossRef]
2. Schmitt, R.W. Double diffusion in oceanography. *Annu. Rev. Fluid Mech.* **1994**, *26*, 255–285. [CrossRef]

3. Ha, S.H.; Kim, G.T. Heat transfer study of double diffusive natural convection in a two-dimensional enclosure at different aspect ratios and thermal Grashof number during the physical vapor transport of mercurous bromide (Hg_2Br_2): Part I. Heat transfer. *J. Korean Cryst. Growth Cryst. Technol.* **2022**, *32*, 16–24.
4. Kelley, D.; Fernando, H.; Gargett, A.; Tanny, J.; Özsoy, E. The diffusive regime of double-diffusive convection. *Prog. Oceanogr.* **2003**, *56*, 461–481. [CrossRef]
5. Gireesha, B.; Archana, M.; Prasannakumara, B.; Gorla, R.R.; Makinde, O.D. MHD three dimensional double diffusive flow of Casson nanofluid with buoyancy forces and nonlinear thermal radiation over a stretching surface. *Int. J. Numer. Methods Heat Fluid Flow* **2017**, *27*, 2858–2878. [CrossRef]
6. Serrano-Arellano, J.; Gijón-Rivera, M.; Riesco-Ávila, J.; Elizalde-Blancas, F. Numerical study of the double diffusive convection phenomena in a closed cavity with internal CO_2 point sources. *Int. J. Heat Mass Transf.* **2014**, *71*, 664–674. [CrossRef]
7. VijayaVenkataRaman, S.; Iniyan, S.; Goic, R. A review of solar drying technologies. *Renew. Sustain. Energy Rev.* **2012**, *16*, 2652–2670. [CrossRef]
8. Alao, F.; Fagbade, A.; Falodun, B. Effects of thermal radiation, Soret and Dufour on an unsteady heat and mass transfer flow of a chemically reacting fluid past a semi-infinite vertical plate with viscous dissipation. *J. Niger. Math. Soc.* **2016**, *35*, 142–158. [CrossRef]
9. Esfe, M.H.; Arani, A.A.A.; Yan, W.-M.; Ehteram, H.; Aghaie, A.; Afrand, M. Natural convection in a trapezoidal enclosure filled with carbon nanotube–EG–water nanofluid. *Int. J. Heat Mass Transf.* **2016**, *92*, 76–82. [CrossRef]
10. Khan, Z.H.; Khan, W.A.; Haq, R.; Usman, M.; Hamid, M. Effects of volume fraction on water-based carbon nanotubes flow in a right-angle trapezoidal cavity: FEM based analysis. *Int. Commun. Heat Mass Transf.* **2020**, *116*, 104640. [CrossRef]
11. Samadifar, M.; Toghraie, D. Numerical simulation of heat transfer enhancement in a plate-fin heat exchanger using a new type of vortex generators. *Appl. Therm. Eng.* **2018**, *133*, 671–681. [CrossRef]
12. Haq, R.U.; Shah, S.S.; Algehyne, E.A. Thermal drift and force convection analysis of nanofluid due to partially heated triangular fins in a porous circular enclosure. *Phys. Scr.* **2021**, *96*, 065701. [CrossRef]
13. Soomro, F.A.; Haq, R.U.; Algehyne, E.A.; Tlili, I. Thermal performance due to magnetohydrodynamics mixed convection flow in a triangular cavity with circular obstacle. *J. Energy Storage* **2020**, *31*, 101702. [CrossRef]
14. Mohammadi, M.; Nassab, S.G. Double-diffusive convection flow with Soret and Dufour effects in an irregular geometry in the presence of thermal radiation. *Int. Commun. Heat Mass Transf.* **2022**, *134*, 106026. [CrossRef]
15. Haq, R.U.; Soomro, F.A.; Wang, X.; Tlili, I. Partially heated lid-driven flow in a hexagonal cavity with inner circular obstacle via FEM. *Int. Commun. Heat Mass Transf.* **2020**, *117*, 104732. [CrossRef]
16. Izadi, S.; Armaghani, T.; Ghasemiasl, R.; Chamkha, A.J.; Molana, M. A comprehensive review on mixed convection of nanofluids in various shapes of enclosures. *Powder Technol.* **2019**, *343*, 880–907. [CrossRef]
17. Bejan, A.; Khair, K.R. Heat and mass transfer by natural convection in a porous medium. *Int. J. Heat Mass Transf.* **1985**, *28*, 909–918. [CrossRef]
18. Goyeau, B.; Songbe, J.-P.; Gobin, D. Numerical study of double-diffusive natural convection in a porous cavity using the Darcy-Brinkman formulation. *Int. J. Heat Mass Transf.* **1996**, *39*, 1363–1378. [CrossRef]
19. Mondal, S.; Sibanda, P. Effects of buoyancy ratio on unsteady double-diffusive natural convection in a cavity filled with porous medium with non-uniform boundary conditions. *Int. J. Heat Mass Transf.* **2015**, *85*, 401–413. [CrossRef]
20. Chamkha, A.J.; Al-Mudhaf, A. Double-diffusive natural convection in inclined porous cavities with various aspect ratios and temperature-dependent heat source or sink. *Heat Mass Transf.* **2008**, *44*, 679–693. [CrossRef]
21. He, B.; Lu, S.; Gao, D.; Chen, W.; Lin, F. Lattice Boltzmann simulation of double diffusive natural convection in heterogeneously porous media of a fluid with temperature-dependent viscosity. *Chin. J. Phys.* **2020**, *63*, 186–200. [CrossRef]
22. Vijaybabu, T. Influence of porous circular cylinder on MHD double-diffusive natural convection and entropy generation. *Int. J. Mech. Sci.* **2021**, *206*, 106625. [CrossRef]
23. Astanina, M.S.; Sheremet, M.A. Numerical study of natural convection of fluid with temperature-dependent viscosity inside a porous cube under non-uniform heating using local thermal non-equilibrium approach. *Int. J. Thermofluids* **2023**, *17*, 100266. [CrossRef]
24. Rashid, U.; Shahzad, H.; Lu, D.; Wang, X.; Majeed, A.H. Non-Newtonian MHD double diffusive natural convection flow and heat transfer in a crown enclosure. *Case Stud. Therm. Eng.* **2023**, *41*, 102541. [CrossRef]
25. Rahman, M.; Saidur, R.; Rahim, N. Conjugated effect of joule heating and magneto-hydrodynamic on double-diffusive mixed convection in a horizontal channel with an open cavity. *Int. J. Heat Mass Transf.* **2011**, *54*, 3201–3213. [CrossRef]
26. Teamah, M.A. Numerical simulation of double diffusive natural convection in rectangular enclosure in the presences of magnetic field and heat source. *Int. J. Therm. Sci.* **2008**, *47*, 237–248. [CrossRef]
27. Kumar, V.; Murthy, S.K.; Kumar, B.R. Influence of MHD forces on Bejan's heatlines and masslines in a doubly stratified fluid saturated Darcy porous enclosure in the presence of Soret and Dufour effects—A numerical study. *Int. J. Heat Mass Transf.* **2018**, *117*, 1041–1062. [CrossRef]
28. Bayareh, M.; Baghoolizadeh, M. An overview of the magnetic field effect on heat transfer and entropy generation in cavities: Application of the second law of thermodynamics and artificial intelligence. *Int. Commun. Heat Mass Transf.* **2024**, *151*, 107238. [CrossRef]

29. Seyyedi, S.M.; Dogonchi, A.; Hashemi-Tilehnoee, M.; Waqas, M.; Ganji, D. Investigation of entropy generation in a square inclined cavity using control volume finite element method with aided quadratic Lagrange interpolation functions. *Int. Commun. Heat Mass Transf.* **2020**, *110*, 104398. [CrossRef]
30. Ali, M.M.; Alim, M.; Ahmed, S.S. Magnetohydrodynamic mixed convection flow in a hexagonal enclosure. *J. Procedia Eng.* **2017**, *194*, 479–486. [CrossRef]
31. Haq, R.U.; Soomro, F.A.; Mekkaoui, T.; Al-Mdallal, Q.M. MHD natural convection flow enclosure in a corrugated cavity filled with a porous medium. *Int. J. Heat Mass Transf.* **2018**, *121*, 1168–1178. [CrossRef]
32. Hussain, S.; Shoeibi, S.; Armaghani, T. Impact of magnetic field and entropy generation of Casson fluid on double diffusive natural convection in staggered cavity. *Int. Commun. Heat Mass Transf.* **2021**, *127*, 105520. [CrossRef]
33. Hamid, M.; Usman, M.; Khan, Z.; Haq, R.; Wang, W. Heat transfer and flow analysis of Casson fluid enclosed in a partially heated trapezoidal cavity. *Int. Commun. Heat Mass Transf.* **2019**, *108*, 104284. [CrossRef]
34. Goodarzi, M.; Safaei, M.; Karimipour, A.; Hooman, K.; Dahari, M.; Kazi, S.; Sadeghinezhad, E. Comparison of the finite volume and lattice Boltzmann methods for solving natural convection heat transfer problems inside cavities and enclosures. *Abstr. Appl. Anal.* **2014**, *2014*, 762184. [CrossRef]
35. Hussain, S.; Schieweck, F.; Turek, S. Efficient Newton-multigrid solution techniques for higher order space–time Galerkin discretizations of incompressible flow. *Appl. Numer. Math.* **2014**, *83*, 51–71. [CrossRef]
36. Retsinis, E.; Papanicolaou, P. A Comparison Between Finite Volume and Finite Difference Method for Lid Driven Cavity Flow. In Proceedings of the 10th GRACM International Congress on Computational Mechanics, Virtual, 5–7 July 2021; pp. 5–7.
37. Shahzad, H.; Ain, Q.U.; Pasha, A.A.; Irshad, K.; Shah, I.A.; Ghaffari, A.; Hafeez, M.B.; Krawczuk, M. Double-diffusive natural convection energy transfer in magnetically influenced Casson fluid flow in trapezoidal enclosure with fillets. *Int. Commun. Heat Mass Transf.* **2022**, *137*, 106236. [CrossRef]
38. Basak, T.; Roy, S.; Paul, T.; Pop, I. Natural convection in a square cavity filled with a porous medium: Effects of various thermal boundary conditions. *Int. J. Heat Mass Transf.* **2006**, *49*, 1430–1441. [CrossRef]

Disclaimer/Publisher's Note: The statements, opinions and data contained in all publications are solely those of the individual author(s) and contributor(s) and not of MDPI and/or the editor(s). MDPI and/or the editor(s) disclaim responsibility for any injury to people or property resulting from any ideas, methods, instructions or products referred to in the content.